J. Appl. Cryst. (1997). **30**, 1026–1035

Diffuse Interfaces and Small-Angle Scattering Intensity Behaviour

SALVINO CICCARIELLO[a]* AND ROGER SOBRY[b]

[a]*Dipartimento di Fisica 'G. Galilei' and Sezione INFM, via Marzolo 8, I-35131 Padova, Italy, and* [b]*Laboratoire de Physique B5, Université de Liège, Sart Tilman, B-4000 Liège, Belgium. E-mail: ciccariello@padova.infn.it*

(*Received 3 January 1997; accepted 3 July 1997*)

Abstract

The contributions corresponding to the Porod, the oscillatory $O(h^{-4})$ and the Kirste–Porod $O(h^{-6})$ terms, present in the asymptotic expansion of the small-angle scattering (SAS) intensities, are numerically evaluated, in the presence of diffuse interfaces generated by different smoothing functions (Gaussian, spherical or Helfand–Tagami). It is shown that SAS experiments are generally unable to distinguish among different profiles, because any smoothing can be made to coincide with another type by scaling its thickness parameter. The oscillatory deviations are observable in the Porod plot of the intensities when the typical distance between parallel diffuse interfaces is greater than 50 Å and the ratio of the thickness to this distance is less than 1/4. The same conclusion applies to the infinite-slit intensities.

1. Introduction

Small-angle scattering (SAS) theory is based on Debye's basic assumption (Debye & Bueche, 1949) that the electron- or scattering-length-density fluctuation of a sample, denoted by $\eta(\mathbf{r})$, can be approximated by a function $\eta_D(\mathbf{r})$ which assumes only N different values: $\eta_1, \ldots, \eta_N$. The regions of the sample where $\eta_D(\mathbf{r})$ is equal to η_i define the ith phase of the sample. (In the following, for the sake of simplicity, it will be assumed that $N = 2$. Moreover, only the electron-density fluctuation will be explicitly referred to.) From the previous assumption it follows that $I(h)/V$,† the properly normalized isotropic pin-hole intensity (see *e.g.* Porod, 1982), asymptotically decreases as $2\pi(n_1 - n_2)^2 S/Vh^4$, with n_1, n_2, S and V denoting the electron densities of the two phases, the area of the interface and the volume of the sample, respectively. This statement is the content of Porod's law (Porod, 1951; Debye *et al.*, 1957). Over the past few decades, considerable effort has been put into finding the corrections to this law. The corrections stem from two limitations in the approach, namely (*a*) Debye's assumption is only an approximation and (*b*) the reported h^{-4} contribution is only the leading monotonically decreasing term. Although both are termed deviations from Porod law, limitations (*a*) and (*b*) have quite different origins and must be corrected simultaneously. Most papers which deal with these issues focus on only one of the two limitations. This paper aims to fill this gap by numerically analyzing the changes in the asymptotic behaviour of the scattered intensity arising from the presence of diffuse interfaces.

† $h = (4\pi/\lambda)\sin(\theta/2)$ denotes the momentum transfer at the scattering angle θ, with λ being equal to the beam particle wavelength.

2. Diffuse interfaces

2.1. *Smoothing functions*

The procedure that can account for the presence of diffuse interfaces was first discussed by Ruland (1971). The results were subsequently applied in order to estimate both the thickness of diffuse regions and the crystallinity of polymer samples (Vonk, 1973; Rathje & Ruland, 1976; Ruland, 1977, 1978). However, even in Ruland's (1987) most recent analysis devoted to the case of fluctuating interfaces, the discussion has been confined to the Porod contribution. Ruland's procedure will be briefly reviewed now and slightly reformulated by using some considerations reported by Ciccariello *et al.* (1988). In general, a sample's electron-density fluctuation can be written as

$$\eta(\mathbf{r}) = \eta_D(\mathbf{r}) + \nu_D(\mathbf{r}). \qquad (1)$$

$\nu_D(\mathbf{r})$ accounts for the deviations, on a microscopic scale, of the electron-density fluctuation of the idealized homogeneous phases compared with that of the real sample. $\nu_D(\mathbf{r})$ presents the same sharp discontinuities (with opposite sign) present in the discrete-valued $\eta_D(\mathbf{r})$ in such a way that the sum on the right-hand side of (1) yields the continuous $\eta(\mathbf{r})$. Clearly, $\eta_D(\mathbf{r})$ represents an idealization rather far from the real electron-density fluctuation. In order to account for the smooth change of the electron-density fluctuation at the real interfaces, which are rather diffuse, Ruland used a suggestion of Hoseman & Bagchi (1962). Ruland assumed that a better idealization of the sample is achieved by approximating its electron-density fluctuation as

$$\eta_{si}(\mathbf{r}) = \int_{R^3} \eta_D(\mathbf{r}+\mathbf{r}_1) w(|\mathbf{r}_1|)\, d\nu_1 = \int_{R^3} \eta_D(\mathbf{r}_1) w(|\mathbf{r}-\mathbf{r}_1|)\, d\nu_1 \quad (2a)$$

where $w(|\mathbf{r}|)$ is a short-range function, depending only on r and obeying the normalization condition

$$\int_{R^3} w(r)\, d\nu = 1. \quad (2b)$$

Equation (2*a*) amounts to saying that at each point $\mathbf{r}$ of the smoothly idealized (si) sample, the electron-density fluctuation is obtained from the Debye idealized one by averaging the latter with the weight function $w(r)$ centred at $\mathbf{r}$. $w(|\mathbf{r}|)$ will be termed the smoothing function. In particular, Ruland considered a Gaussian form for $w(|\mathbf{r}|)$, *i.e.*

$$w_G(|\mathbf{r}|) = (\pi^{1/2}\sigma_G)^{-3} \exp(-r^2/\sigma_G^2), \quad (3)$$

where $2\sigma_G$ roughly represents the thickness of the diffuse regions around the interfaces. One is reminded that Ruland considered the variance of the smoothing function as the measure of the interface thickness. This amounts to putting $\sigma_R = \sigma_G/(2)^{1/2}$ in equation (3), with σ_R coinciding with Ruland's quantity σ. Clearly, the choice of the smoothing functions is rather arbitrary. A quite reasonable choice might also be

$$w_{Sp}(|\mathbf{r}|) = 3/(4\pi\sigma_{Sp}^3)\theta(\sigma_{Sp} - r). \quad (4)$$

This amounts to averaging over a sphere of radius σ_{Sp} [hence the subscript Sp on the left-hand side (l.h.s.) and right-hand side (r.h.s.) of (4)]. With this smoothing, the thickness of the interface is exactly $2\sigma_{Sp}$ and $\eta_{si}(\mathbf{r})$ is rigorously constant for the points away from the sharp interface more so than σ_{Sp}. It is noted that the actual form of the electron density inside the diffuse region depends on both the smoothing and the shape of the sharp interface. As an illustration, we have evaluated these profiles around a spherical surface with radius R. After putting $r \equiv R + x$, $\hat{x} = x/\sigma$ and $\hat{R} \equiv R/\sigma$ and taking $n_1 = 1$ and $n_2 = 0$, the expressions resulting from (2*a*) after substituting (3) or (4) will be denoted, respectively, by $\eta_G(\hat{x}, \hat{R})$ and $\eta_{Sp}(\hat{x}, \hat{R})$. These expressions are

$$\eta_G(\hat{x}, \hat{R}) = \tfrac{1}{2}\left(\Phi(-\hat{x}) + \Phi(2\hat{R}+\hat{x}) + \left\{ \frac{\exp[-(2\hat{R}+\hat{x})^2] - \exp(-\hat{x}^2)}{(\pi)^{1/2}(\hat{R}+\hat{x})} \right\} \right), \quad 1 \le \hat{R}, \quad -\hat{R} \le x, \quad (5a)$$

and

$$\eta_{Sp}(\hat{x}, \hat{R}) = \begin{cases} 1, & \text{if } -\hat{R} \le \hat{x} \le -1 \\ \frac{1}{4}\left[\hat{R}^3(1-\cos\alpha)^2(2+\cos\alpha) + (1-\cos\beta)^2 \times (2+\cos\beta)\right], & \text{if } -1 \le \hat{x} \le 1 \\ 0, & \text{if } 1 \le \hat{x}. \end{cases} \quad (5b)$$

where $\hat{R} > 1$ and

$$\cos\alpha \equiv \frac{2\hat{R}^2 + \hat{x}^2 + 2\hat{R}\hat{x} - 1}{2\hat{R}(\hat{x}+\hat{R})},$$

$$\cos\beta \equiv \frac{1 + \hat{x}^2 + 2\hat{R}\hat{x}}{2(\hat{x}+\hat{R})}.$$

Function Φ in equation (5*a*) denotes the error function (Abramowitz & Stegun, 1972), while the r.h.s. of (5*b*) is the overlapping volume between two spheres with radii R and σ and with their centres at distance r. It is noted that the limits of equations (5*a*) and (5*b*), as $\hat{R} \to \infty$, yield the density profiles around a planar surface for the Gaussian and the spherical smoothing, respectively. Fig. 1 shows the plots of (5*a*) and (5*b*) for three typical values of $\hat{R}$. For each smoothing, it is evident that the electron-density profiles also depend on the considered sharp interface. In fact, the profiles change as the sphere radius changes, although the changes are not dramatic. More-

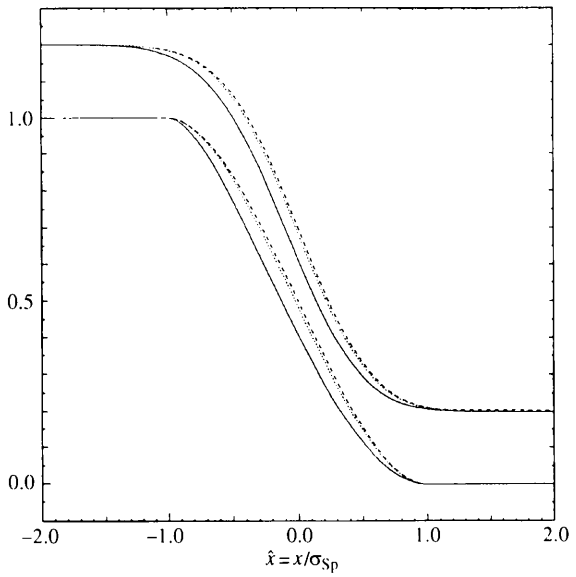

Fig. 1. The upper and lower sets of three curves show the electron-density profiles, generated by the Gaussian and spherical smoothing functions, respectively, along a radial direction orthogonal to a spherical surface. The continuous, dotted and broken lines, in the lower set of curves, represent the plot of $\eta_{Sp}(\hat{x}, \hat{R})$, defined by equation (5*b*), with $\hat{R} = 2$, 10 and 100, respectively. The upper three curves represent the plots of $\eta_G[\hat{x}(2/5)^{1/2}, \hat{R}(2/5)^{1/2}]$ [see equation (5*a*)], shifted vertically by 0.2. [The reason the variables of this function have been scaled by a factor $(2/5)^{1/2}$ is explained before equation (22*a*).]

over, comparison of the two sets of profiles shows that, despite the fact that smoothing functions (3) and (4) appear quite different, the resulting density profiles behave rather similarly. Slight differences are only observable near $\hat{x} = \pm 1$, where the Gaussian profiles look smoother than the spherical ones. This result indicates that the experimental study of the details of electron-density profiles in the transition regions is not an easy task and that different smoothing functions are often almost equivalent.

For completeness and later reference, two further smoothing functions, widely used in the study of polymer samples, will now be recalled. The first, introduced by Vonk (1973) in the one-dimensional case, assumes that the electron-density profile between two phases of a sample changes linearly in the diffuse region. In the three-dimensional case, this condition is ensured by the following smoothing function

$$w_{\mathrm{SpS}}(r) = \delta(r - \sigma_{\mathrm{SpS}})/(4\pi\sigma_{\mathrm{SpS}}^2), \tag{6}$$

where $\delta(\cdot)$ denotes the (one-dimensional) Dirac function. The use of smoothing (6) amounts to averaging $\eta_D(\mathbf{r})$ over a spherical surface (hence the subscript SpS) of radius σ_{SpS} in order to obtain the corresponding smoothed idealized electron-density fluctuation $\eta_{\mathrm{si}}(\mathbf{r})$. [It is also noted that σ_{SpS} is related to Vonk's quantity E and to quantity t, used by Hashimoto *et al.* (1977), by the relation $E = t = 2\sigma_{\mathrm{SpS}}$.] The other density profile looks physically more sound because it was obtained by Helfand & Tagami (1971, 1972) for polymer samples, on the basis of the mechanical statistical theory of inhomogeneous fluids (Percus, 1982). In fact, Helfand and Tagami showed that, across a planar phase boundary (orthogonal to the x axis), the density profile for a polymer is $0.5[1 - \tanh(x/\sigma)]$. It is rather straightforward to show that the corresponding isotropic three-dimensional smoothing function is

$$w_{\mathrm{HT}}(r) = \frac{1}{2\pi\sigma_{\mathrm{HT}}^3}\frac{\sigma_{\mathrm{HT}}}{r}\frac{\sinh(r/\sigma_{\mathrm{HT}})}{\cosh^3(r/\sigma_{\mathrm{HT}})}, \tag{7}$$

where σ_{HT} denotes the thickness of the transition region.

2.2. *Smoothing and scattered intensity expression*

Let us now analyze the functional expression of scattered intensities in the presence of diffuse interfaces. By any of the idealizations discussed previously, equation (1) becomes

$$\eta(\mathbf{r}) = \eta_{\mathrm{si}}(\mathbf{r}) + \nu_{\mathrm{si}}(\mathbf{r}). \tag{8}$$

Since $\eta_{\mathrm{si}}(\mathbf{r})$ is now a continuous function, the same occurs for $\nu_{\mathrm{si}}(\mathbf{r})$ which accounts for the differences between the electron-density fluctuation of the sample and that of the smoothly idealized sample described by $\eta_{\mathrm{si}}(\mathbf{r})$. These differences are mainly present in the phases' internal regions, though they may also occur at the diffuse interfaces when the smoothing adopted does not exactly reproduce the electron-density fluctuation on the borders of the real sample's phases. By definition, the average of $\eta(\mathbf{r})$, performed throughout the sample, is equal to zero, *i.e.* $\langle \eta(\cdot) \rangle_V = 0$. Hence, in choosing $\eta_D(\mathbf{r})$, it is required that $\langle \eta_D(\cdot) \rangle_V = 0$. Then, from (2*a*) and (2*b*), it follows that $\langle \eta_{\mathrm{si}}(\cdot) \rangle_V = 0$. This condition also holds true for $\langle \nu_{\mathrm{si}}(\cdot) \rangle_V$, as it can easily be proven starting from (8). Hence

$$\langle \eta_{\mathrm{si}}(\cdot) \rangle_V = 0 \qquad \text{and} \qquad \langle \nu_{\mathrm{si}}(\cdot) \rangle_V = 0. \tag{9}$$

The isotropic component of the observed scattered intensity (divided by Thomson's electron form factor) is related to $\tilde{\eta}(\mathbf{h})$, the Fourier transform (FT) of $\eta(\mathbf{r})$ defined as

$$\tilde{\eta}(\mathbf{h}) = \int_{R^3} \exp(i\mathbf{h} \cdot \mathbf{r})\eta(\mathbf{r})\, \mathrm{d}v, \tag{10}$$

by

$$I(h) = (4\pi)^{-1} \int \mathrm{d}\hat{\omega} \left|\tilde{\eta}(h\hat{\omega})\right|^2. \tag{11}$$

with $\hat{\omega} = \mathbf{h}/h$. The FT of (8), by equation (2*a*), yields

$$\tilde{\eta}(\mathbf{h}) = \tilde{\eta}_D(\mathbf{h})\tilde{w}(h) + \tilde{\nu}_{\mathrm{si}}(\mathbf{h}), \tag{12}$$

where the central-function property of $w(r)$ has been used. (The tilde over the symbol of a function denotes the FT of the latter.) The substitution of (12) into (11) yields

$$I(h) = I_{\mathrm{si}}(h) + \mathcal{I}_{\mathrm{bck}}(h), \tag{13}$$

where

$$I_{\mathrm{si}}(h) \equiv \tilde{w}^2(h) I_D(h), \tag{14a}$$

$$I_D(h) \equiv (4\pi)^{-1} \int \mathrm{d}\hat{\omega} \left|\tilde{\eta}_D(h\hat{\omega})\right|^2, \tag{14b}$$

$$\mathcal{I}_{\mathrm{bck}}(h) \equiv \mathcal{I}_{\mathrm{mfl}}(h) + \mathcal{I}_{\mathrm{int}}(h), \tag{14c}$$

$$\mathcal{I}_{\mathrm{mfl}}(h) \equiv (4\pi)^{-1} \int \mathrm{d}\hat{\omega} \left|\tilde{\nu}_{\mathrm{si}}(h\hat{\omega})\right|^2, \tag{14d}$$

$$\mathcal{I}_{\mathrm{int}}(h) \equiv (2\pi)^{-1} \tilde{w}(h) \int \mathrm{d}\hat{\omega}\, \Re\left[\tilde{\eta}_D(h\hat{\omega})\overline{\tilde{\nu}_{\mathrm{si}}(h\hat{\omega})}\right]. \tag{14e}$$

Here, $\Re$ and the overbar, respectively, denote the real part and the complex conjugate. These equations deserve some attention. $I_{\mathrm{si}}(h)$ is the intensity scattered by the idealized sample, consisting of homogeneous phases with diffuse boundaries or, in other words, by the sample characterized by the electron-density fluctuation $\eta_{\mathrm{si}}(\mathbf{r})$ defined by equation (2*a*). In contrast, $\mathcal{I}_{\mathrm{bck}}(h)$ simply represents the correction to be added to $I_{\mathrm{si}}(h)$ in order to recover the observed intensity $I(h)$. Since $\mathcal{I}_{\mathrm{bck}}(h)$ is mainly related to $\nu_{\mathrm{si}}(\mathbf{r})$ (the remaining microscopic fluctuation of the electron density), it is commonly referred to as the background contribution. According to (14*c*), $\mathcal{I}_{\mathrm{bck}}(h)$ consists of two contributions. The first, $\mathcal{I}_{\mathrm{mfl}}(h)$, is

the isotropic component of the intensity scattered by an ideal sample characterized by the electron density $\nu_{si}(\mathbf{r}) = \eta(\mathbf{r}) - \eta_{si}(\mathbf{r})$, which can be considered as an electron-density fluctuation taking place on a quite small length scale. Hence, this contribution will be referred to as the microscopic fluctuation (mfl) intensity. In contrast, the second contribution $\mathcal{I}_{int}(h)$ is an interference (int) term which cannot be interpreted as an intensity because it can be negative for some h values. Different ways of approximating $\mathcal{I}_{bck}(h)$ and their implications for the relevant best-fit results have been thoroughly discussed by Luzzati *et al.* (1961), Ruland (1971), Vonk (1973), Koberstein *et al.* (1980) and Roe (1982). A further approximation, based on rather general arguments, will be discussed later. With any of these $\mathcal{I}_{bck}(h)$ approximations at hand, $I_{si}(h)$ is immediately obtained from the observed intensity $I(h)$ by equation (13). Then, the intensity scattered by the sample idealized with sharp interfaces is obtained by writing (14*a*) as

$$I_D(h) = [I(h) - \mathcal{I}_{bck}(h)]/\tilde{w}^2(h). \qquad (14f)$$

3. Asymptotic behaviour

In principle, relation (14*f*) also allows one to determine $I_D(h)$ in the region of very large values of h. At this point, the corrections to limitation (*b*), reported in §1, come into play. In fact, over the past few years, it has been shown that the asymptotic expansion of $I_D(h)$ contains a lot of information on the geometry of the interphase surfaces, because the coefficients of the asymptotic expansion are related to some well defined geometric features of the sharp interfaces, as will be briefly recalled now. By developing a procedure first put forward by Schmidt (1965) (see also Wu & Schmidt, 1971, 1974), it has been shown recently that the general expression of the leading $O(h^4)$ asymptotic term (lat) is as follows (Ciccariello, 1991*a*)

$$I_{D,lat}(h) = \sum_{i=0}^{M} \frac{\mathcal{A}_i \cos(\delta_i h) + \mathcal{B}_i \sin(\delta_i h)}{h^4}. \qquad (15)$$

Here, δ_i denotes the distance between the portions of the interface which are parallel to each other. One is reminded that two portions Σ_1 and Σ_2 of the interface surface $\mathcal{S}$ are said to be parallel, at a relative distance δ, when each point P_1 of Σ_1 is at distance δ from a point P_2 of Σ_2 along the straight line going through P_1 and P_2 and orthogonal to Σ_1 and Σ_2. Stated differently, if Σ_1 is considered as the configuration of a wavefront at a given instant, Σ_2 represents the configuration of the wavefront after the latter has travelled through a distance δ. In this way, Σ_2 results from the envelope of the spheres (with radius δ) centred on Σ_1. Now, each of these spheres, in a neighbourhood of its tangency point with Σ_2, can lie on either one side or both sides of Σ_2. In the first case, the parallelism is said to be elliptical, in the second hyperbolic. Spheres and cylinders are paramount examples of surfaces which are elliptically or hyperbolically parallel to themselves, respectively, with a relative distance equal to their diameters. Elliptical and hyperbolical parallelism are responsible for the factors $\cos(\delta h)$ and $\sin(\delta h)$, respectively, in equation (15). The integral expressions of the $\mathcal{A}_i$'s and $\mathcal{B}_i$'s are given by equations (3.17), (3.18), (3.13) and (3.14) of Ciccariello (1991*a*). Their explicit expression for some particularly simple geometries such as hollow spheres, cylinders and tori was reported by Ciccariello (1991*b*). The well known Porod contribution is contained in (15), because each surface is elliptically parallel to itself for the distance $\delta_0 = 0$. For this distance, in fact, $\mathcal{A}_0 = 2\pi(\eta_1 - \eta_2)^2 S$ results and the Porod–Debye contribution

$$\mathcal{P}_{PD}/h^4 \equiv 2\pi(n_1 - n_2)^2 S/h^4 \qquad (16)$$

is obtained. (n_1, n_2 and S, as previously reported, denote the electron densities of the two homogeneous phases and the area of the interphase surface, respectively.) It is also recalled that Kirste & Porod (1962) obtained the general expression of the contribution monotonously decreasing as h^{-6} in the case of smooth interfaces. Its expression is

$$\mathcal{K}_{KP}/h^6 \equiv \pi(n_1 - n_2)^2 S[3\langle H^2\rangle_S - \langle\kappa\rangle_S]/h^6, \qquad (17)$$

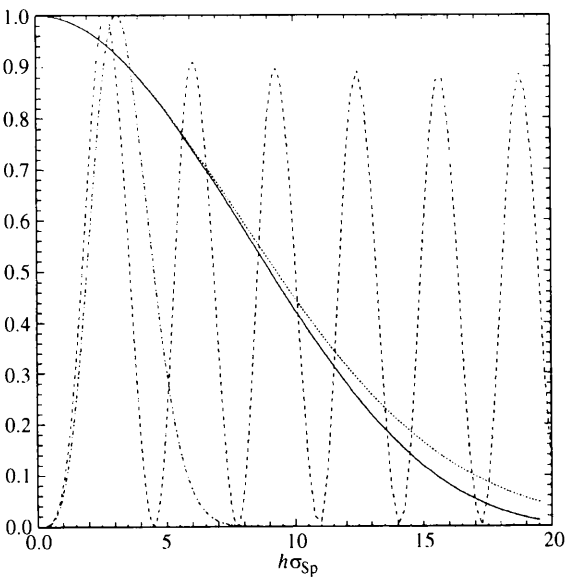

Fig. 2. The continuous and dotted lines represent, respectively, $\tilde{w}^2_{Sp}(\sigma_{Sp}h)$ and $\tilde{w}^2_G[(2/5)^{1/2}\sigma_{Sp}h]$ *versus* $5\sigma_{Sp}h$, while the broken and dash–dotted lines represent $(\sigma_{Sp}h)^4\tilde{w}^2_{Sp}(\sigma_{Sp}h)$ and $(\sigma_{Sp}h)^4\tilde{w}^2_G \times[(2/5)^{1/2}\sigma_G h]$ *versus* $\sigma_{Sp}h$. For the latter two curves, the dimensionless values of the reported vertical scale must be multiplied by 13.52 and 10.16, respectively.

where $\langle H^2\rangle_S$ and $\langle\kappa\rangle_S$ denote, respectively, the averages of the squared mean curvature and the Gaussian curvature of the interface throughout the latter. The corrections to the value of $\mathcal{K}_{KP}$, arising from the presence of vertices and sharp curvilinear edges, have been discussed recently by Sobry *et al.* (1991) and Ciccariello & Sobry (1995). For smooth interfaces also, the contributions monotonously decreasing as h^{-8} and h^{-10} have been explicitly evaluated by Wu & Schmidt (1971) and Ciccariello (1995), respectively. Their expressions, however, are so involved as to make their practical application quite difficult. Schmidt (1965) pointed out the existence of oscillatory terms decreasing as $h^{-4.5}$ in the case of right cylinders. Hence, oscillatory contributions decreasing as $h^{-\alpha}$ with $\alpha > 4$ should, in general, be expected but their expressions are as yet unknown. Therefore, in the following only the leading asymptotic contributions, given by equation (15) and the Kirste–Porod contribution $\mathcal{K}_{KP}/h^6$ [see equation (17)], will be taken into account. Even with this drastic simplification, the behaviour of $h^4 I_D(h)$ is far from being a constant in the asymptotic region, in contrast to what is commonly assumed. Indeed, oscillatory deviations superimposed to a constant plus a monotonously h^{-2} decreasing contribution are generally to be expected in the Porod plot [*i.e.* $h^4 I(h)$ *versus* h] of the intensities.

4. Numerical analysis

4.1. *Pin-hole collimation*

Owing to the presence of diffuse interfaces and to the unknown $I_{bck}(h)$ contribution, one wonders whether these oscillations can really be observed and, in the affirmative case, how sensitive they are to the smoothing function. These problems will now be discussed.

First of all, it is sensible to assume that $I_D(h)$ is fairly well approximated by its asymptotic expansion once h has become sufficiently large to make

$$hD_{min} \geq 2\pi, \tag{18}$$

D_{min} denoting the smallest distance between the interfaces. This condition ensures that $\delta_i > D_{min}$ for $i = 1, \ldots, M$ and that $2\sigma < D_{min}$. The squared three-dimensional FTs of $w_G(r)$ and of $w_{Sp}(r)$, respectively, are

$$\tilde{w}_G^2(\sigma_G h) = \exp(-\sigma_G^2 h^2/2) \tag{19}$$

and

$$\tilde{w}_{Sp}^2(\sigma_{Sp} h) = 9[h\sigma_{Sp}\cos(h\sigma_{Sp}) - \sin(h\sigma_{Sp})]^2/(h\sigma_{Sp})^6. \tag{20}$$

At large h values, the asymptotic behaviour of $\tilde{w}_G^2(\sigma_G h)$ is radically different from that of $\tilde{w}_{Sp}^2(\sigma_{Sp} h)$ because the former decreases as $\exp(-\sigma_G^2 h^2/2)$ and the latter as h^{-4} (leaving aside the oscillatory factors). At very small h values, the expansions of (19) and (20) are, respectively, given by

$$\tilde{w}_G^2(x_G) \simeq 1 - \frac{x_G^2}{2} + \frac{x_G^4}{8} - \frac{x_G^6}{48} + \frac{x_G^8}{384} + \ldots, \quad x_G \equiv \sigma_G h, \tag{21a}$$

$$\tilde{w}_{Sp}^2(x_{Sp}) \simeq 1 - \frac{x_{Sp}^2}{5} + \frac{3x_{Sp}^4}{175} - \frac{4x_{Sp}^6}{4725} + \frac{2x_{Sp}^8}{72765} + \ldots, \quad x_{Sp} \equiv h\sigma_{Sp}. \tag{21b}$$

These can be made to coincide for terms up to $O(h^2)$ by setting

$$\sigma_G = \sigma_{Sp}(2/5)^{1/2}. \tag{22a}$$

With this scaling, squared FTs (19) and (20) of the Gaussian and the spherical smoothing differ less than 0.5% throughout the h range where $h\sigma_{Sp} \leq 1$, while their difference monotonously increases to 9% as $h\sigma_{Sp}$ increases to 2. This property also holds true with Vonk's and Helfand–Tagami's smoothing, *i.e.* equations (6) and (7), respectively. In fact, the squares of the three-dimensional FTs of the latter coincide with those obtained by Vonk (1973) and Helfand & Tagami (1972) in the one-dimensional case and are given, respectively, by

$$\tilde{w}_{SpS}^2(h) = \sin^2(h\sigma_{SpS})/(h\sigma_{SpS})^2 \simeq 1 - (h\sigma_{SpS})^2/3 + \ldots$$

and

$$\tilde{w}_{HT}^2(h) = (h\pi\sigma_{HT}/2)^2/\sinh^2(h\pi\sigma_{HT}/2) \simeq 1 - \frac{(\pi\sigma_{HT}h)^2}{12} + \ldots.$$

The thickness scaling, given, respectively, by

$$E = t = 2\sigma_{SpS} = 2\sigma_{Sp}(3/5)^{1/2} = 2(3/2)^{1/2}\sigma_G = (12)^{1/2}\sigma_R \tag{22b}$$

and

$$\sigma_{HT} = \sigma_{Sp}(12/5)^{1/2}/\pi \simeq 0.5\sigma_{Sp}, \tag{22c}$$

ensures that these smoothing functions are practically indistinguishable from the spherical one in the range $h\sigma_{Sp} \leq 2$. From these considerations, it is concluded that by an appropriate scaling of the thickness parameter each of the four considered smoothing functions becomes indistinguishable from the others when the considered h values are such that $h\sigma_{Sp} < 2$. At larger $h\sigma_{Sp}$ values, the differences increase and become quite evident when $h\sigma_{Sp} > 2\pi$. This fact is evident from Fig. 2 which, for simplicity, shows only the results relevant to the Porod term for the spherical and Gaussian smoothing. Furthermore, polynomial approximation (21*b*) ensures a

relative error less than 0.143% [1.51% if the term $O(x^8)$ is neglected] in the range $x \equiv h\sigma_{Sp} \leq 2$. Let $[h_m,h_M]$ denote the h range where it is believed that $I_D(h)$ can be represented by its asymptotic expression. For the most accurate SAS experiments, $h_M \simeq 0.4$ Å^{-1}. Hence, the largest thickness which can be determined independently from the precise form of the smoothing function (leaving aside the trivial scaling mentioned above) is $\sigma_{Sp,max} = 2/0.4 = 5$ Å. With the choice $h_m = 0.1$ Å^{-1}, $D_{min} = 2\pi/0.1 \simeq 60$ Å results and the ratio $\tau \equiv \sigma_{Sp}/D_{min}$ is bounded by $5/60 \simeq 0.1$. Thus (with the spherical smoothing), only when the thickness does not exceed 5 Å and $\tau \leq 0.1$ is it possible to have an unambiguous Debye idealization (in the sense that it is independent of the details of the diffuse regions at the interface) and to have at hand an h range where the analysis of the asymptotic behaviour of $I_D(h)$ can be attempted. Concerning the oscillatory contributions, it is noted that they are not obscured by the smoothing, provided τ is not too large. This is evident from Fig. 3 where, as an illustration, only the contribution resulting from the spherical smoothing of the $\cos(h\delta)/h^4$ term has been considered. The figure, in particular, shows the corresponding Porod plots, *i.e.* those of $\tilde{w}^2_{Sp}(h\delta\tau_{Sp})\cos(h\delta)$ *versus* $h\delta$, for different values of $\tau_{Sp} = \sigma_{Sp}/\delta$. The oscillations are quite evident in the region $h\delta > 2\pi$ even with $\tau_{Sp} = 1/4$, a value greater than the upper bound considered above. The discrepancy between $\tilde{w}^2_{Sp}(h\delta\tau_{Sp})\cos(h\delta)$ and $\tilde{w}^2_G[h\delta\tau_G(2/5)^{1/2}]\cos(h\delta)$ increases with τ_{Sp} and with $h\delta$. At $h\delta = 20$, it is 5% and 80% for $\tau_{Sp} = 0.1$ and 0.2, respectively. In these cases, the corresponding $h\sigma_{Sp}$ values turn out to be equal to 2 and 4, respectively. It is concluded that, with the pin-hole collimation, when the Kirste and the Kirste–Porod terms are able (unable) to discriminate among different profiles, the oscillatory terms also are (are not) sensitive to the smoothing.

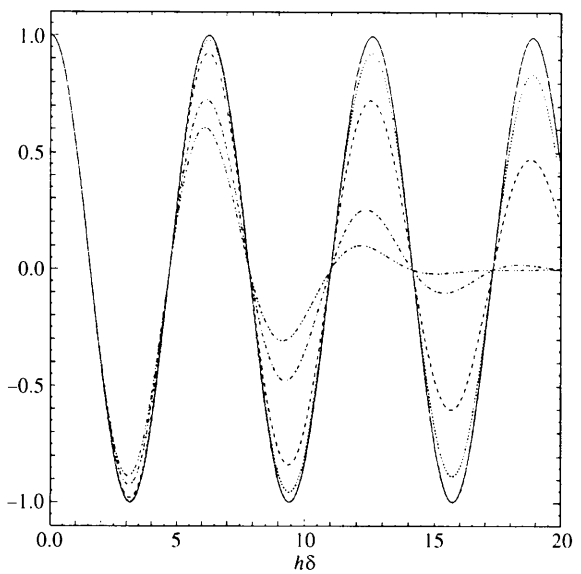

Fig. 3. Pin-hole collimation: Porod plots of the diffuse cosine oscillatory contribution. The continuous, dotted, broken, dash–dotted and dot–dot–dashed lines are the plots of $\tilde{w}^2_{Sp}(\tau_{Sp}h\delta)\cos(h\delta)$ for $\tau_{Sp} \equiv \sigma_{Sp}/\delta = 0.01$, 0.05, 0.1, 0.2 and 0.25, respectively.

However, in order to perform the asymptotic analysis, it is important to estimate the behaviour of $\mathcal{I}_{bck}(h)$ in the range $h \leq h_M$ since this contribution must be subtracted from $I(h)$ in order to determine $I_{si}(h)$ [see equation (13)]. Consider first $\mathcal{I}_{mfl}(h)$. It is reasonable to assume that $\nu_{si}(\mathbf{r})$ is rather small and endowed of continuous derivatives throughout the sample. Moreover, the typical size of the domains where $\nu_{si}(\mathbf{r})$ is appreciably different from zero is expected to be much smaller than D_{min}. For this reason, $\nu_{si}(\mathbf{h})$ ought to be fairly well approximated by the first terms of its expansion at $\mathbf{h} = 0$ in the range $h < h_m$

$$\tilde{\nu}_{si}(\mathbf{h}) \simeq h^2[-\nu_2 + h^2\nu_4], \tag{23a}$$

where

$$\nu_2 \equiv (1/3!)\int_V r^2\nu_{si}(\mathbf{r})\,d\nu, \tag{23b}$$

$$\nu_4 \equiv (1/5!)\int_V r^4\nu_{si}(\mathbf{r})\,d\nu. \tag{23c}$$

Then, for $h \leq h_M$, from (14*d*) it follows that

$$\mathcal{I}_{mfl}(h) \simeq h^4[\nu_2^2 - 2h^2\nu_2\nu_4]. \tag{24}$$

An estimate of $\mathcal{I}_{int}(h)$, though less accurate than the one just obtained, can be derived as follows. After substituting (23*a*) in the integrand on the r.h.s. of (14*e*), this becomes

$$(2\pi)^{-1}\tilde{w}(h)h^2[-\nu_2 + h^2\nu_4]\int d\hat{\omega}\,\Re\tilde{\eta}_D(h\hat{\omega}). \tag{25a}$$

On the one hand,

$$|\int \Re\tilde{\eta}_D(h\hat{\omega})|d\hat{\omega} \leq \int |\tilde{\eta}_D(h\hat{\omega})|\,d\hat{\omega}. \tag{25b}$$

On the other hand, at least in first approximation, (14*b*) can be written as

$$I_D(h) \simeq [\langle|\tilde{\eta}_D(h\cdot)|\rangle_\Omega]^2$$

where the average has been performed over all possible orientations $\hat{\omega}$ of $\mathbf{h}$. From this relation it follows that

$$\langle|\tilde{\eta}_D(h\cdot)|\rangle_\Omega \simeq I_D^{1/2}(h). \tag{25c}$$

Equations (25*a*) and (14*e*) show that $\mathcal{I}_{int}(h)$ is $O(h^2)$ as $h \to 0$. Ruland (1971) has shown that the corrections to the scattered intensity arising from the electron-density fluctuations internal to the phases must be positive at small h values. Hence, by combining (25*a*), (25*b*) and (25*c*), it can be assumed that

$$\int d\hat{\omega}\,\Re\tilde{\eta}_D(h\hat{\omega}) \simeq -2I_D^{1/2}(h)\,\mathrm{sign}(\nu_2),$$

because, in this way, equation (25*a*) becomes

$$2h^2[|\nu_2| - h^2\nu_4\,\mathrm{sign}(\nu_2)]\tilde{w}(h)I_D^{1/2}(h) \qquad (26)$$

and the positiveness is ensured at very small h values. For continuity, it will now be assumed that this equation holds true throughout the SAS explored h range. Combining (24) and (26), the following estimate of $\mathcal{I}_{\mathrm{bck}}(h)$

$$\mathcal{I}_{\mathrm{bck}}(h) = 2h^2[|\nu_2| - h^2\nu_4\,\mathrm{sign}(\nu_2)]\tilde{w}(h)I_D^{1/2}(h) + h^4(\nu_2^2 - 2h^2\nu_2\nu_4) \qquad (27)$$

is obtained. It is stressed that this contribution is $O(h^2)$ at very small h by condition (9), while in the asymptotic range $h_m \le h \le h_M$ it develops a constant contribution, as is commonly assumed in the analysis of SAS intensities (Luzzati *et al.*, 1961), because in this range $I_D^{1/2}(h) \simeq I_{D,\mathrm{lat}}^{1/2}(h) \propto h^{-2}$ and $\tilde{w}(h) \simeq \tilde{w}(0) = 1$.

4.2. *Infinite-slit collimation*

The intensity observed with this collimation will be denoted by $J(h)$. It is obtained from the pin-hole one by the integral transform

$$J(h) = 2\int_0^\infty I[(h^2 + t^2)^{1/2}]\mathrm{d}t = 2h\int_1^\infty \frac{I(ht)t}{(t^2-1)^{1/2}}\mathrm{d}t. \qquad (28)$$

The same integral transform applied to $I_{\mathrm{si}}(h)$, $I_D(h)$, $\mathcal{I}_{\mathrm{bck}}(h)$, $\mathcal{I}_{\mathrm{mfl}}(h)$ and $\mathcal{I}_{\mathrm{int}}(h)$, given by equations (14*a*)–(14*e*), will respectively define the quantities $J_{\mathrm{si}}(h)$, $J_D(h)$, $\mathcal{J}_{\mathrm{bck}}(h)$, $\mathcal{J}_{\mathrm{mfl}}(h)$ and $\mathcal{J}_{\mathrm{int}}(h)$.

We are now interested to see if the asymptotic analysis can be performed directly on the observed infinite-slit intensity $J(h)$ in order to avoid the desmearing of the latter. In the case of sharp interfaces, $J(h)$ reduces to $J_D(h)$. The asymptotic behaviour of this quantity is obtained by applying integral transform (28) to each term defining $I_{D,\mathrm{lat}}(h)$. In this way, immediately one sees that the Porod and the Kirste–Porod contributions, respectively, become

$$\pi\mathcal{P}_{\mathrm{PD}}/2h^3 \qquad (29a)$$

and

$$3\pi\mathcal{K}_{\mathrm{KP}}/8h^5, \qquad (29b)$$

where $\mathcal{P}_{\mathrm{PD}}$ and $\mathcal{K}_{\mathrm{KP}}$ have been defined in equations (16) and (17). The cos and sin contributions respectively become

$$\frac{\pi\mathcal{A}}{2h^3}\varphi_{\cos}(h\delta) \qquad (30a)$$

and

$$\frac{\pi\mathcal{B}}{2h^3}\varphi_{\sin}(h\delta), \qquad (30b)$$

where

$$\varphi_{\cos}(h\delta) \equiv \frac{4}{\pi}\int_1^\infty \frac{\cos(h\delta t)}{t^3(t^2-1)^{1/2}}\mathrm{d}t \qquad (31a)$$

and

$$\varphi_{\sin}(h\delta) \equiv \frac{4}{\pi}\int_1^\infty \frac{\sin(h\delta t)}{t^3(t^2-1)^{1/2}}\mathrm{d}t. \qquad (31b)$$

Functions $\varphi_{\cos}(h\delta)$ and $\varphi_{\sin}(h\delta)$ can be expressed as hypergeometric functions and, in this way, it is possible to know both their small and large $h\delta$ asymptotic expansions. The details of this analysis will be reported elsewhere because, from a numerical point of view, these expressions are not particularly useful. A simple and accurate algebraic approximation of $\varphi_{\cos}(h\delta)$ has already been given by Ciccariello & Benedetti (1986) [where $\varphi_{\cos}(h\delta)$ is denoted by $\varphi_0(h\delta)$].

In the presence of diffuse interfaces, the leading asymptotic terms of $J_{\mathrm{si}}(h)$ in the region $hD_{\min} > 2\pi$ are obtained from the definition

$$J_{\mathrm{si}}(h) = 2h\int_1^\infty \frac{\tilde{w}^2(ht)I_D(th)t}{(t^2-1)^{1/2}}\mathrm{d}t \qquad (32)$$

by substituting $I_D(h)$ with its asymptotic expansion. From equations (16) and (17) it follows that the Porod and the Kirste–Porod terms respectively become

$$\frac{\pi\mathcal{P}_{\mathrm{PD}}}{2h^3}\varphi_{a,3}(h\sigma_a) \qquad (33a)$$

and

$$\frac{3\pi\mathcal{K}_{\mathrm{KP}}}{8h^5}\varphi_{a,5}(h\sigma_a), \qquad (33b)$$

where

$$\varphi_{a,3}(h\sigma_a) \equiv (4/\pi)\int_1^\infty \frac{\tilde{w}_a^2(h\sigma_a t)}{t^3(t^2-1)^{1/2}}\mathrm{d}t, \qquad (34a)$$

$$\varphi_{a,5}(h\sigma_a) \equiv (16/3\pi)\int_1^\infty \frac{\tilde{w}_a^2(h\sigma_a t)}{t^5(t^2-1)^{1/2}}\mathrm{d}t. \qquad (34b)$$

Here index a labels the different smoothing. Moreover, $\varphi_{a,3}(h\sigma_a)$ and $\varphi_{a,5}(h\sigma_a)$ have been defined in such a way that $\varphi_{a,3}(0) = \varphi_{a,5}(0) = 1$. Similarly, with the infinite-slit collimation, each of the oscillatory damped contributions, related either to the elliptical or the hyperbolic parallel interfaces, gives rise, respectively, to

$$\frac{\pi\mathcal{A}}{2h^3}\varphi_{a,\cos}(h\delta, \tau_a) \quad \text{or to} \quad \frac{\pi\mathcal{B}}{2h^3}\varphi_{a,\sin}(h\delta, \tau_a), \qquad (35a, b)$$

where

$$\varphi_{a,\cos}(h\delta, \tau_a) \equiv \frac{4}{\pi}\int_1^\infty \frac{\cos(h\delta t)\tilde{w}_a^2(\delta h\tau_a t)}{t^3(t^2-1)^{1/2}}\,dt, \qquad (36a)$$

$$\varphi_{a,\sin}(h\delta, \tau_a) \equiv \frac{4}{\pi}\int_1^\infty \frac{\sin(h\delta t)\tilde{w}_a^2(\delta h\tau_a t)}{t^3(t^2-1)^{1/2}}\,dt. \qquad (36b)$$

In these relations, $\tau_a \equiv \sigma_a/\delta$. Moreover, $\varphi_{a,\cos}(h\delta, 0) = \varphi_{\cos}(h\delta)$ and $\varphi_{a,\sin}(h\delta, 0) = \varphi_{\sin}(h\delta)$. With the Gaussian smoothing, it is possible to evaluate explicitly $\varphi_{G,3}(h\sigma_G)$ and $\varphi_{G,5}(h\sigma_G)$. The first, evaluated by Ruland (1971), reads

$$\varphi_{G,3}[(2)^{1/2}x] = [2xe^{-x^2}/(\pi)^{1/2} + (1-2x^2)\mathrm{Er\,fc}(x)]; \qquad (37)$$

the second is

$$\varphi_{G,5}[(2)^{1/2}x] = \tfrac{1}{3}[2xe^{-x^2}(3-2x^2)/(\pi)^{1/2} + (3-4x^2+4x^4)\mathrm{Er\,fc}(x)] \qquad (38)$$

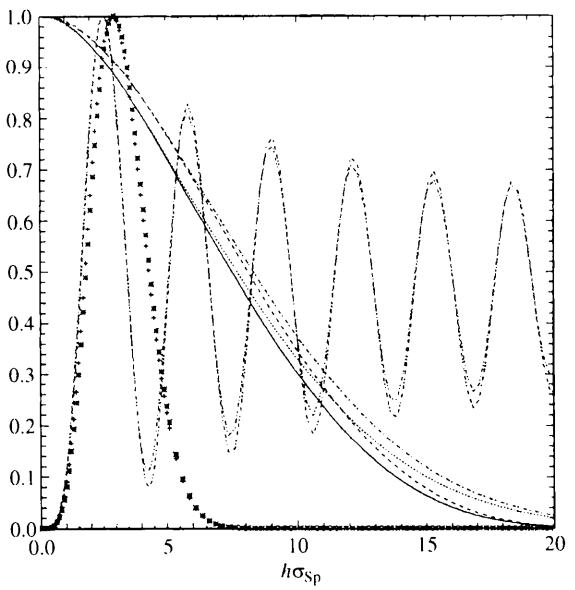

Fig. 4. Infinite-slit collimation: the continuous and dotted lines are the plots of $\varphi_{G,3}[(2/5)^{1/2}\sigma_{Sp}h]$ and $\varphi_{Sp,3}(\sigma_{Sp}h)$ *versus* $5\sigma_{Sp}h$ and represent the Porod plots of the Porod contribution in the presence of a spherical or Gaussian smoothing function, respectively. Similarly, the broken and dash–dotted lines are the plots of $\varphi_{G,5}[(2/5)^{1/2}\sigma_{Sp}h]$ and $\varphi_{Sp,5}(\sigma_{Sp}h)$ (*versus* $5\sigma_{Sp}h$), related to the Kirste–Porod term. The remaining curves show the behaviour at larger h values. In particular, the oscillatory broken curves are the plots of $(\sigma_{Sp}h)^4\varphi_{Sp,3}(\sigma_{Sp}h)$ and $(\sigma_{Sp}h)^4\varphi_{Sp,5}(\sigma_{Sp}h)$ (characterized by wider oscillations) *versus* $\sigma_{Sp}h$, while the symbols + and * are those of $(\sigma_{Sp}h)^4\varphi_{G,3}[(2/5)^{1/2}\sigma_{Sp}h]$ and $(\sigma_{Sp}h)^4\varphi_{G,5}[(2/5)^{1/2}\sigma_{Sp}h]$. For the latter four curves, the dimensionless values of the vertical scale must be multiplied by 6.01, 7.16, 8.11 and 9.61, respectively.

where Er fc(x) is the so-called complementary error function (see *e.g.* Abramowitz & Stegun, 1972). With the Gaussian smoothing, integrals (36) can only be determined numerically. With the spherical smoothing, both integrals (34) and (36) have to be evaluated numerically. These tasks have explicitly been carried out by using appropriate subroutines of the NAG library. Figs. 4, 5 and 6 show the corresponding results. In particular, Fig. 4

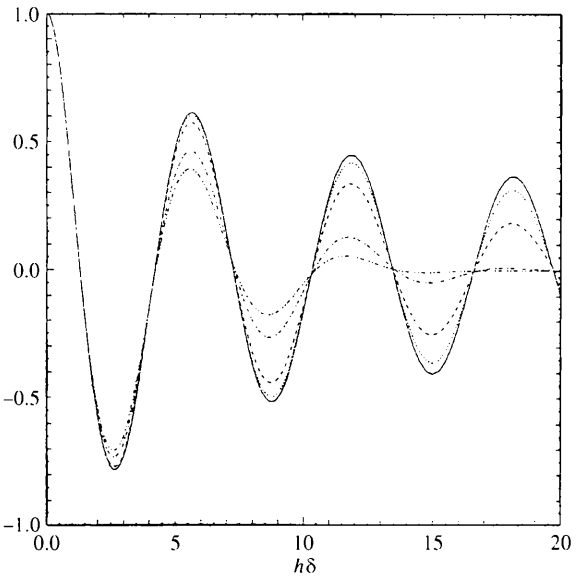

Fig. 5. Infinite-slit collimation: the continuous, dotted, broken, dash–dotted and dot–dot–dashed lines are the plots of $\varphi_{Sp,\cos}(\sigma_{Sp}h,\tau_{Sp})$ for τ_{Sp} = 0.01, 0.05, 0.1, 0.2 and 0.25, respectively.

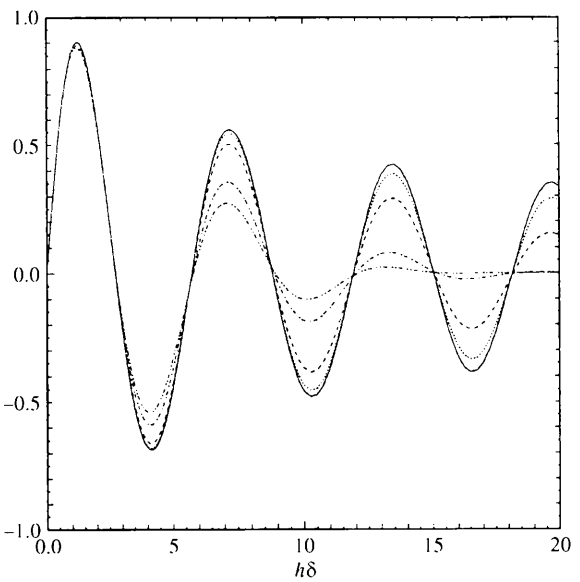

Fig. 6. Infinite-slit collimation: the continuous, dotted, broken, dash–dotted and dot–dot–dashed lines are the plots of $\varphi_{Sp,\sin}(\sigma_{Sp}h,\tau_{Sp})$ for τ_{Sp} = 0.01, 0.05, 0.1, 0.2 and 0.25, respectively.

shows the plots of $\varphi_{G,3}(h\sigma_G)$ (continuous line), $\varphi_{Sp,3}(h\sigma_{Sp})$ (dotted line), $\varphi_{G,5}(h\sigma_G)$ (broken line) and $\varphi_{Sp,5}(h\sigma_{Sp})$ (dash–dotted line) [with $\sigma_G = \sigma_{Sp}(2/5)^{1/2}$] *versus* $h\sigma_{Sp}$. As in the pin-hole case, the two smoothing functions almost coincide up to $h\sigma_{Sp} = 2$. For this value in particular, their relative differences are 9% and 8%, respectively. As these values are larger than those found in the pin-hole case, it is concluded that with the infinite-slit collimation, the Porod and the Kirste–Porod terms are more sensitive to the actual form of the smoothing than in the pin-hole case. For greater $h\sigma_{Sp}$ values, the two smoothing functions become quite different, but in order to observe this effect it is necessary to enlarge the vertical scale or, as shown in the figure, to plot a different quantity. These differences, however, can hardly be detected, because the intensity has become so small as to make the signal unrecognizable from the noise. Thus, the greater sensitivity, observed with the slit collimation, is in practice confined to a smaller h range. Fig. 5 shows $\varphi_{Sp,cos}(h\delta,\tau_{Sp})$ *versus* $h\delta$ for the values 0.01, 0.05, 0.1, 0.2, 0.25 and 0.5 of the ratio $\tau_{Sp} \equiv \sigma_{Sp}/\delta$. Fig. 6 shows the plots of $\varphi_{Sp,sin}(h\delta,\tau_{Sp})$ for the same τ_{Sp} values. The oscillation presence is evident from the two figures. Besides, as τ_{Sp} increases, the positions of the nodes are practically fixed as in the pin-hole case, though the amplitudes of the oscillations are noticeably more damped. Nonetheless, despite the damping, the oscillations are still quite evident in the asymptotic range $h\delta > 2\pi$ when $\tau_{Sp} < 1/4$. With the Gaussian smoothing, both $\varphi_{G,cos}(h\delta, \tau_G)$ and $\varphi_{G,sin}(h\delta,\tau_G)$ practically coincide with the corresponding expression relevant to the spherical smoothing, once $\sigma_G = (2/5)^{1/2}\sigma_{Sp}$. Their difference, in fact, cannot be observed with the vertical scale of the reported figures throughout the range $h\delta < 20$. Hence, with the slit collimation, the oscillatory contributions are much less sensitive to the density profile than in the pin-hole case. In practice, with the slit collimation, only the Porod and the Kirste–Porod terms can discriminate the most appropriate density profile.

In any case, these results allow us to conclude that, as with the infinite-slit collimation, the oscillatory deviations of the intensities can be observed in the Porod plot when $D_{min} > 50$ Å and the thickness of the diffuse region is such that $\tau_{Sp} < 1/4$. Of course, for this really to happen, it is necessary for the ratio of the area of the parallel surface to that of the total interface not to be too small for the amplitude of the oscillations to be observed in comparison with the height of the Porod plateau. It is difficult to make this statement more quantitative. Moreover, the asymptotic analysis of the tail of an observed slit intensity requires that the contribution owed to $\mathcal{J}_{bck}(h)$ be taken into account. To this end, it is important to give the analytic expression of this contribution. Clearly, many of the considerations reported before equation (23*a*) also apply to $\mathcal{J}_{bck}(h)$. In particular, condition (9) ensures that $\mathcal{J}_{bck}(0) = 0$. Hence, similar to the $\mathcal{I}_{bck}(h)$ expression, it appears reasonable that

$$\mathcal{J}_{bck}(h) = \beta_0 + \beta_1 h^2 \tag{39}$$

in the asymptotic range $[h_m,h_M]$, even though, in this case, relating coefficients β_0 and β_1 to the first momenta of $\nu_{si}(\mathbf{r})$ appears to be a dubious procedure which, therefore, will not be reported. In any case, the best fit of the observed slit intensity can be performed by approximating $\mathcal{J}_{bck}(h)$ with (39) and $\mathcal{J}_{si}(h)$ with the sum of (33), (34) and some of the contributions (35) and (36). The actual number of terms to be considered depends on the number of free parameters which can unambiguously be fitted and on the reliability of the resulting values.

5. Conclusion

It has been shown that in favourable circumstances the presence of diffuse interfaces does not obscure the presence of oscillatory deviations in the Porod plot. Observation of these oscillations requires τ, the ratio of the thickness of the diffuse interfaces to the distance between parallel surfaces, to be no larger than 1/4 and the typical interface distance to be >50 Å. Concerning the possibility of discriminating among different density profiles (aside from obvious scaling), this is possible only when $\tau_{Sp} \geq 0.1$ by examining the behaviour of the Porod and the Kirste–Porod terms. Besides, for $0.1 < \tau_{Sp} \leq 0.25$, the oscillatory contributions show some sensitivity to precise density-profile form only with pin-hole collimation.

It should be stressed that the practical application of the former expressions leads to considerably weaker results. Indeed, one can expect that throughout the range $\tau_{Sp} \leq 1/4$, the best fits of the tails of the observed SAS intensities, due to experimental errors and to the rather large number of parameters involved, turn out to be equally satisfactory, whatever the smoothing function. Hence, the scaling of the thickness parameter, in practice, can always be applied. On the one hand, this implies that the numerical analyses can be carried out with the most convenient density profile. Of course, the resulting thickness value makes sense only when the profile used in the best-fit procedure is specified. Besides, this value can be converted into the 'true' one by a simple scaling, when the 'true' profile function relevant to the considered sample is known. This is so for polymers where smoothing (7), for the reason reported before (7), can be be considered as the true one. On the other hand, these considerations show the density profile cannot be uniquely determined by analyzing only the tails of the SAS intensities.† In contrast, when one deals with the

† With further assumptions, of course, it is possible to say more. For instance, by depicting the interface region as a third phase characterized by an average electron density n_3, Benedetti & Ciccariello (1994) have shown that it is possible to get reliable estimates of the third phase's thickness and of n_3 when D and 2σ obey the constraints $D \geq 80$ Å and $2\sigma = \delta \geq 10$ Å.

SAS intensity observed throughout the explored h range, then D_{min} can be less than 50 Å and the τ value can be larger than 1/4. In these cases, at least in principle, it is possible to determine the most accurate smoothing function among those considered. However, in order to carry out this analysis, the analytical expression of $I_D(h)$ has to be known throughout the explored h range, a condition rather hard to meet. Finally, the presence of an appreciable correction to the apparent interfacial thickness, recently pointed out by Semenov (1994) in the case of anisotropic samples, could make the analysis of these samples more interesting for the determination of the density profiles.

Financial support from MURST through 40% and 60% Funds and from CGRI (Commisariat Général aux Relations Internationales) is gratefully acknowledged.

References

Abramowitz, M. & Stegun, I. A. (1972). *Handbook of Mathematical Functions*. New York: Dover.
Benedetti, A. & Ciccariello, S. (1994). *J. Appl. Cryst.* **27**, 249–256.
Ciccariello, S. (1991*a*). *Phys. Rev.* A**44**, 2975–2984.
Ciccariello, S. (1991*b*). *J. Appl. Cryst.* **24**, 509–515.
Ciccariello, S. (1995). *J. Math. Phys. (NY)*, **36**, 219–246.
Ciccariello, S. & Benedetti, A. (1986). *J. Appl. Cryst.* **19**, 195–197.
Ciccariello, S., Goodisman, J. & Brumberger, H. (1988). *J. Appl. Cryst.* **21**, 117–128.
Ciccariello, S. & Sobry, R. (1995). *Acta Cryst.* A**51**, 60–69.
Debye, P., Anderson, H. R. & Brumberger, H. (1957). *J. Appl. Phys.* **28**, 679–683.
Debye, P. & Bueche, A. M. (1949). *J. Appl. Phys.* **20**, 518–525.
Hashimoto, T., Todo, A., Itoi, H. & Kawai, H. (1977). *Macromolecules*, **10**, 377–384.
Helfand, E. & Tagami, Y. (1971). *Polym. Lett.* **9**, 741–746.
Helfand, E. & Tagami, Y. (1972). *J. Chem. Phys.* **56**, 3592–3601.
Hoseman, R. & Bagchi, S. N. (1962). *Direct Analysis of Diffraction by Matter*. Amsterdam: North-Holland.
Kirste, R. & Porod, G. (1962). *Kolloid-Z.* **184**, 1–7.
Koberstein, J. T., Morra, B. & Stein, R. S. (1980). *J. Appl. Cryst.* **13**, 34–45.
Luzzati, V., Witz, J. & Nicolaieff, A. (1961). *J. Mol. Biol.* **3**, 367–371.
Percus, J. K. (1982). *Liquid State of Matter: Fluids, Simple and Complex*, edited by E. W. Montroll & J. L. Lebowitz, pp. 31–140. Amsterdam: North-Holland.
Porod, G. (1951). *Kolloid-Z.* **124**, 83–87; **125**, 51–56.
Porod, G. (1982). *Small Angle X-ray Scattering*, edited by O. Glatter & O. Kratky, ch. 1. London: Academic Press.
Rathje, J. & Ruland, W. (1976). *Colloid Polym. Sci.* **254**, 358–370.
Roe, R.-J. (1982). *J. Appl. Cryst.* **15**, 182–189.
Ruland, W. (1971). *J. Appl. Cryst.* **4**, 70–73.
Ruland, W. (1977). *Colloid Polym. Sci.* **255**, 417–427.
Ruland, W. (1978). *Colloid Polym. Sci.* **256**, 932–936.
Ruland, W. (1987). *Macromolecules*, **20**, 87–93.
Schmidt, P. W. (1965). *J. Math. Phys. (NY)*, **6**, 424–431.
Semenov, A. N. (1994). *Macromolecules*, **27**, 2732–2735.
Sobry, R., Ledent, J. & Fontaine, F. (1991). *J. Appl. Cryst.* **24**, 516–525.
Vonk, C. G. (1973). *J. Appl. Cryst.* **6**, 81–86.
Wu, H. & Schmidt, P. W. (1971). *J. Appl. Cryst.* **4**, 224–231.
Wu, H. & Schmidt, P. W. (1974). *J. Appl. Cryst.* **7**, 131–146.